THE JOURNAL OF PHYSICAL CHEMISTRY A

Article

pubs.acs.org/JPCA

Monotrimethylene-Bridged Bis-*p*-phenylenediamine Radical Cations and Dications: Spin States, Conformations, and Dynamics

Michal Zalibera,*[,†,‡] Almaz S. Jalilov,[§,∥] Stefan Stoll,[⊥] Ilia A. Guzei,[§] Georg Gescheidt,*[,†] and Stephen F. Nelsen[§]

[†]Institute of Physical and Theoretical Chemistry, Graz University of Technology, Technikerstraße 4/I, A-8010 Graz, Austria

[‡]Institute of Physical Chemistry and Chemical Physics, Faculty of Chemical and Food Technology, Slovak University of Technology, SK-81237 Bratislava, Slovakia

[§]Department of Chemistry, University of Wisconsin, Madison, 1101 University Avenue, Madison, Wisconsin 53706-1396, United States

[⊥]Department of Chemistry, University of Washington, Seattle, Washington 98195-1700, United States

[∥]Department of Chemistry, Northwestern University, Evanston, Illinois 60208-3113, United States

Supporting Information

ABSTRACT: The properties of *p*-phenylenediamine- (PD-) based systems substantially depend on the molecular topology. The singly bridged PD analogues HMPD and OMPD in which the PD rings are connected by a flexible linker reveal particular electronic properties in their radical cations and dications. The EPR and UV−vis spectra of $HMPD^{2+\bullet\bullet}$ were found to be exceptionally temperature-sensitive, following a change from the extended conformation (doublet−doublet state) predominant at room temperature to the π-stacked conformation (singlet state) prevailing at dry-ice temperature. Changing the single bridge from $(CH_2)_3$ to dimethylated $CH_2CMe_2CH_2$ in $OMPD^{2+\bullet\bullet}$ causes considerably less of the π-stacked conformation to be present at low temperature as a result of the steric interactions with the methyl groups of the bridge. In contrast to $HMPD^{2+\bullet\bullet}$ and $OMPD^{2+\bullet\bullet}$, in which the positive charges are localized separately in each $PD^{+\bullet}$ ring, in the extended conformation, exchange of the electron ("hole hopping") between the two PD units (fast at the time scale of EPR experiments) was observed for $HMPD^{+\bullet}$ and $OMPD^{+\bullet}$. This process slows in a reversible manner with decreasing temperature, thus forming the radical cation with the unpaired electron spin density predominantly on one PD core, at low temperatures. Accordingly, a subtle balance between conformational changes, electron delocalization, and spin states could be established.

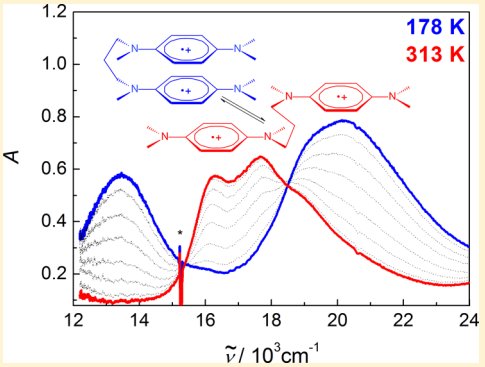

1. INTRODUCTION

Phenylamino and *p*-phenylenediamine (PD) moieties have been utilized as common motifs in a variety of functional materials.[1−7] A particularly attractive feature of PD derivatives is their advantageous oxidation potential, making them excellent electron donors. In addition, oxidation of PDs is accompanied by characteristic electronic absorptions in the visible range.[8−10] These properties are closely connected with the mode of the connection between the PD units. It is straightforward that the electron delocalization within a conjugated π-system is an important characteristic in polyaniline. However, when PDs are connected by alkyl bridges, the through-bond and through-space interactions,[11−13] which depend on the molecular topology, become significant.[14−16]

Such phenomena were illustrated in our previous work on oxidized *p*-phenylenediamine(PD) dimers, such as the doubly $(CH_2)_3$-bridged [5,5]paracyclophanes **1(R)**, (R = Me and Et; see Chart 1),[17] which displayed clearly differing conformations depending on the charge (neutral, cation, dication) and the substitution pattern.[17,18] Notably, neutral π-stacking has an important dispersion component,[19,20] and it is known that local density approximation (LDA) calculations do not treat dispersion correctly. However, surprisingly, the relative amounts of these conformations, which are significantly different for $\mathbf{1(Me)}^{2+}$ and $\mathbf{1(Et)}^{2+}$, are predicted in the correct order by LDA calculations, and time-dependent LDA calculations allow the assignment of the optical absorption bands for both dications.

The structures of paramagnetic stages could be established from the electron paramagnetic resonance (EPR) and electron−nuclear double resonance (ENDOR) spectroscopic data.[21] Another study examined the compound analogous to $\mathbf{1(Me)}^{2+}$ that has centrally methylated $CH_2CMe_2CH_2$ bridges, $\mathbf{2}^{2+}$.[22] Steric effects, which are also predicted properly by LDA calculations, cause an unsymmetrical conformation with one of its PD^+ units *syn* and the other one *anti* (abbreviated *uns*) to be

Received: October 22, 2012
Revised: January 22, 2013
Published: January 22, 2013

   dx.doi.org/10.1021/jp3104358 | *J. Phys. Chem. A* 2013, 117, 1439−1448

Chart 1

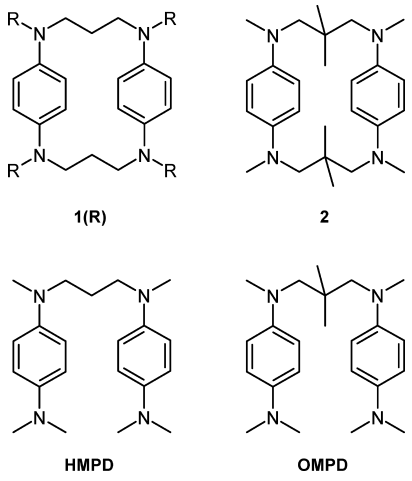

Scheme 1. Preparation of HMPD and OMPD

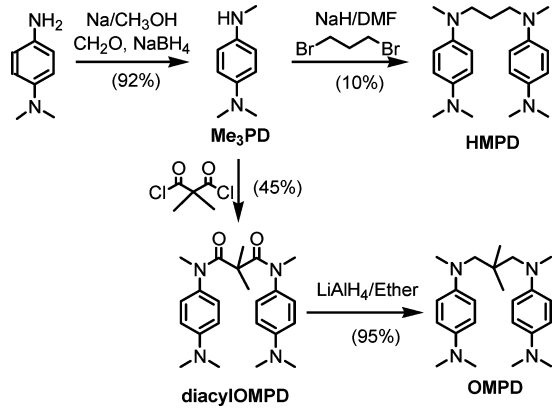

much more stable relative to the symmetrical conformations with both PD^+ units either in the doubly syn or anti conformations. This work also provided the first available crystal structure of a monocation in this series, that of the solvated $\mathbf{2}^+B(C_6F_5)_4^-$. The large counterion proved necessary for isolation of the monocation, as attempted isolation of the SbF_6^- monocation salt resulted in electron-transfer disproportionation and isolation of the dication salt. Comparison of the crystal structures of $\mathbf{2}^+$ and $\mathbf{2}^{2+}$, where both are in the *uns* conformation, demonstrated significantly closer approach of the PD^+ units of $\mathbf{2}^{2+}$, implying that multicenter π-stacking is more efficient for the singlet $\mathbf{2}^{2+}$ than for the doublet $\mathbf{2}^+$ and that spin-pairing allows better bonding even at closer-than-van-der-Waals (vdW) distances despite the Coulomb repulsion at the less-than-vdW distances of $\mathbf{2}^{2+}$.

These results indicate that both molecular topology and chemical environment, particularly association with counterions, determine the electronic properties of PD-based systems. Moreover, for (multiply) charged, (radical) cationic, forms different spin states (singlet, doublet, triplet, etc.) have to be taken into account.[23,24]

The mono-C_3-bridged compounds *N,N′*-di(*n*-dimethylaminophenyl)-*N,N′*-dimethyl-1,3-propanediamine (HMPD) and *N,N′*-di(*p*-dimethylaminophenyl)-2,2-dimethyl-1,3-propanediamine (OMPD) introduced in this work offer an even extended palette of aspects: The presence of only one connecting bridge in HMPD and OMPD allows a substantially broader conformational flexibility than in the more constrained cyclophanes **1(R)** and **2**.[17,18,21,22] Accordingly, aside from π-stacking, several additional conformations for which π-stacking cannot occur are much more likely to be populated, and dynamic phenomena can be expected. These effects were followed in the one- and two-electron oxidized stages of HMPD and OMPD. This was achieved by combining cyclovoltammetric measurements with UV−vis and EPR spectroscopies.

2. EXPERIMENTAL SECTION

2.1. Materials. The routes used to prepare HMPD, which was similar to a literature method,[25] and OMPD are shown in Scheme 1.

N,N,N′-Trimethyl-p-phenylenediamine (Me_3PD). Na (3.5 g, 150 mmol) was dissolved in 75 mL of dry methanol, and *N,N*-dimethyl-*p*-phenylenediamine (7.3 g, 54 mmol) was added. The resulting solution was added to 2.1 g (70.2 mmol) of paraformaldehyde in 50 mL of methanol and stirred for 5 h at room temperature. Next, 2 g (54 mmol) of $NaBH_4$ was added to the reaction mixture, which was refluxed for 1 h. After evaporation of solvent, 50 mL of 1 M aqueous KOH was added, and the mixture was extracted with ethyl acetate. The residual crude compound was passed through a silica column with hexane/ethylacetate/triethylamine (50:25:4 by volume) as the eluent to yield 7.4 g of **1** (92%) as a brown oil after solvent removal. ^1H NMR ($CDCl_3$): δ (ppm) 6.75 (m, 2H, Ar−H), 6.26 (m, 2H, Ar−H), 3.60 (s, H, N−H), 2.82 (s, 6H, N−CH_3), 2.80 (s, 3H, N−CH_3).

N,N′-Di(n-dimethylaminophenyl)-N,N′-dimethyl-1,3-propanediamine (HMPD). *N,N,N′*-Trimethyl-*p*-phenylenediamine (**1**) (7.4 g, 22 mmol) and sodium hydride (60% in mineral oil, 2.2 g) were dispersed in dimethylformamide (DMF, 36 mL) and stirred at 55 °C. After 1 h, the temperature was raised to 120 °C, and a solution of 1,3-dibromopropane (5.05 g, 48 mmol) in DMF (200 mL) was added dropwise over a period of 2 h; the resultant solution was stirred for another 2 h. The solution was then poured into hot brine, and the precipitates were collected by suction filtration. The crude product was purified by flash chromatography on silica gel with hexane/ethylacetate/triethylamine (100:10:1 by volume) to give 0.311 g, 13%. Mp 58−60 °C. ^1H NMR ($CDCl_3$, 300.135 MHz): δ (ppm) 6.76 (q, 8H, Ar−H), 3.23 (t, 4H, N−CH_2), 2.83 (s, 18H, N−CH_3), 1.79 (quint, 2H, N−CH_2−CH_2−). HR-MS: TOF MS ES+ calcd $[M + H]^+$ = 341.2700, measured $[M + H]^+$ = 341.2684 (4.7 ppm).

N,N′-Di(n-dimethylaminophenyl)-2,2-dimethyl-1,3-propanediamide (diacylOMPD in Scheme 1). To a mixture of suspended *N,N,N′*-trimethyl-*p*-phenylenediamine (**1**) (7.0 g, 20 mmol) and 5.88 g (70 mmol) of dimethylmalonyl chloride in ethyl acetate (50 mL) was added a solution of 2.63 g (15.6 mmol) of triethylamine in 20 mL of ethyl acetate dropwise over 10 min, and the reaction mixture stirred at room temperature for 10 h. The solution was then poured into 50 mL of water, and the organic phase was separated, dried over $MgSO_4$, and evaporated under reduced pressure to yield 5 g (45%) of crude gray solid. The crude product was purified by flash chromatography on silica gel with hexane/ethylacetate/triethylamine (100:10:1 by volume) to give 4.5 g, 40%. Mp 80−90 °C. ^1H NMR ($CDCl_3$, 300.137 MHz): δ (ppm) 6.76 (q, 8 H, Ar−H), 2.92 (s, 12H, N−CH_3), 0.77 (s, 6H, C−CH_3) ppm. HR-MS: TOF MS ES+ calcd $[M + H]^+$ = 397.2599, measured $[M + H]^+$ = 397.2587 (3.0 ppm).

dx.doi.org/10.1021/jp3104358 | J. Phys. Chem. A 2013, 117, 1439−1448

N,N′-Di(p-dimethylaminophenyl)-2,2-dimethyl-1,3-propanediamine (OMPD). To a suspension of 1.06 g (70 mmol) of $LiAlH_4$ in ether (40 mL) was added *N,N′*-di(n-dimethylaminophenyl)-3,3′-dimethyl-2,4-propanediamide (2.7 g, 20 mmol) by portions over 20 min, and the mixture was refluxed for 4 h. Then, 1 mL of water was added to the reaction mixture, the mixture was filtered, and the organic phase was evaporated under reduced pressure to yield 0.25 g (15%) of crude dark oil. The crude product was purified by flash chromatography on silica gel with hexane/ethylacetate/triethylamine (100:10:1 by volume) to give 0.15 g, 10%. ^{1}H NMR ($CDCl_3$, 300.137 MHz): δ (ppm) 6.78 (d, 8 H, Ar−H), 3.15 (s, 4H, N−CH_2-C), 2.91 (s, 6H, N−CH_3), 2.84 (s, 12H, N−CH_3), 1.06 (s, 6H, C−CH_3) ppm. HR-MS: TOF MS ES+ calcd $[M + H]^+$ = 369.3013, measured $[M + H]^+$ = 369.3021 (2.2 ppm).

Sample Preparation for EPR. Dichloromethane (CH_2Cl_2), acetonitrile (CH_3CN), silver nitrate ($AgNO_3$, puriss, p.a. ACS 99.5%), silver perchlorate ($AgClO_4$ anhydrous, 97%), and ferrocene (Fc, purum ≥98%) were obtained from Fluka. Methanol (anhydrous, 99.8%), [bis(trifluoroacetoxy)iodo]-benzene (PIFA, 97%), and nitrosonium hexafluoroantimonate ($NOSbF_6$, 99.9% trace-metal basis) were obtained from Sigma-Aldrich and were used as received. Tetrabutylammonium perchlorate (TBAP, puriss, electrochemical grade, Fluka, dried under reduced pressure at 340 K for 24 h prior to use) was used as the supporting electrolyte.

2.2. Electrochemistry. Voltammograms were obtained with a PG 284 potentiostat (HEKA, Germany) in a small volume electrochemical cell built from a 1.5 mL vial and three electrodes. Platinum wires served as working and counter electrodes and a silver wire was used as the pseudoreference electrode. Sample solutions with approximate concentration of 1 mM, prepared with 0.1 M TBAP supporting electrolyte in CH_3CN, were purged with Ar for 15 min before each experiment. Cyclic voltammograms (CV) were recorded at the scan rate of 100 mV s^{-1}. Squarewave voltammograms (SWV) were obtained with 50 mV pulse amplitude, 50 ms pulse width and 5 mV step potential. Fc was used as internal potential standard and all potentials are referred to the Fc/Fc^+ couple.

2.3. Spectroelectrochemistry. Solutions for the in situ spectroelectrochemical experiments consisted of the sample studied in a concentration of 1−2 mM and 0.2 M TBAP as the supporting electrolyte in CH_3CN. They were purged with Ar for 15 min and filled into a flat EPR spectroelectrochemcial cell described earlier.[26,27] A three-electrode arrangement with laminated Pt mesh as working, Pt wire as counter and Ag wire as pseudoreference electrode was used. EPR spectra were recorded with an X-band EMX EPR spectrometer (Bruker, Germany) equipped with the optical resonator ER 4104OR. The UV−vis spectrometer PC2000 (Ocean Optics, Inc.) was connected to the EPR resonator via light guides for the simultaneous detection of UV−vis spectra. A PG 284 potentiostat (HEKA, Germany) was used for the potential control.

2.4. Spectroscopic Measurements. In addition to electrochemical oxidation several different chemical oxidants were used to obtain the diradical dications and the radical cations of the monobridged PD derivatives. The diradical dications we prepared by the oxidation of the sample with a 2fold excess of PIFA or $NOSbF_6$ in CH_2Cl_2 or methanol. While the oxidation with PIFA yielded the $HMPD^{2+}$ in solution the use of $NOSbF_6$ resulted in the precipitation of the $HMPD^{2+}(SbF_6)_2$ salt from CH_2Cl_2. The radical monocations of HMPD and OMPD were generated by the oxidation with a substochiometric amount of PIFA in CH_2Cl_2 and methanol and by a trace amount of $AgClO_4$ or $AgNO_3$ in CH_2Cl_2. Additionally the monocations were also obtained via the comproportionation reaction of the dication solutions with a ∼10 fold excess of the neutral HMPD and OMPD. EPR and UV−vis spectrometers mentioned above were used for spectroscopic measurements and the ER 4111VT unit (Bruker, Germany) served for temperature control in the *in situ* EPR/UV−vis experiments. O_2 was removed from the CH_2Cl_2 samples by three successive freeze−pump−thaw cycles and from the methanol samples by the rigorous purging of the solutions with Ar for >15 min. The detected EPR spectra were analyzed and simulated employing WinEPR and SimFonia, (Bruker) Winsim2002.[28] For isotropic EPR spectra displaying dynamic exchange phenomena, EasySpin was used.[29] To model intramolecular exchange, EasySpin implements density matrix theory in Liouville space with the appropriate exchange operator.[30−32]

2.5. X-ray Crystallography. Single crystals of the dication salt $HMPD(SbF_6)_2$ were prepared by dissolving the dication salts in acetonitrile and the resulting clear solutions were overlaid with small amount of the mixture of diethylether and acetonitrile, which was again overlaid with excess diethylether. The solvent mixture was kept in a refrigerator at −20 °C for several days to give purple colored single crystals. A single crystal with approximate dimensions 0.11 × 0.08 × 0.05 mm^3 was selected from mother liquor deposited in an indentation of a glass microscope slide situated in a special argon-filled container at approximately −25 °C and attached to the tip of a ″tennis-racquet″-shaped MiTeGen MicroMount. The crystal was mounted in a stream of cold nitrogen at 100(1) K and centered in the X-ray beam by using a video camera. The crystal evaluation and data collection were performed on a Bruker Quazar SMART APEXII diffractometer with Mo K_α (λ = 0.71073 Å) radiation and the diffractometer to crystal distance of 4.96 cm. The initial cell constants were obtained from three series of ω scans at different starting angles. Each series consisted of 12 frames collected at intervals of 0.5° in a 6° range about ω with the exposure time of 10 s per frame. The reflections were successfully indexed by an automated indexing routine built in the APEXII program suite. The final cell constants were calculated from a set of 9729 strong reflections from the actual data collection. The data were collected by using the full sphere data collection routine to survey the reciprocal space to the extent of a full sphere to a resolution of 0.8 Å. A total of 21758 data were harvested by collecting 4 sets of frames with 0.5° scans in ω and φ with exposure times of 60 s per frame. These highly redundant data sets were corrected for Lorentz and polarization effects.

The systematic absences in the diffraction data were consistent for the space groups $P2_1$ and $P2_1/m$. The *E*-statistics was inconclusive. Based on prior knowledge and work on related structures space group $P2_1$ was selected. It yielded chemically reasonable and computationally stable results of refinement.[33,34]

A successful solution by the direct methods provided most non-hydrogen atoms from the *E*-map. The remaining non-hydrogen atoms were located in an alternating series of least-squares cycles and difference Fourier maps.

dx.doi.org/10.1021/jp3104358 | J. Phys. Chem. A 2013, 117, 1439−1448

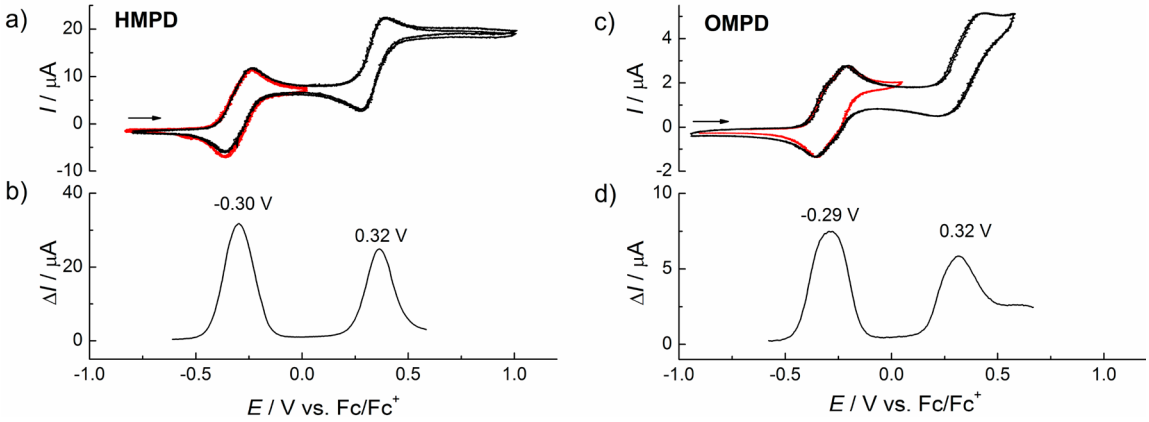

Figure 1. (a) CV of HMPD in 0.1 M TBAP/CH_3CN solution using a Pt working electrode (scan rate = 100 mV s^{-1}). Two successive scans are shown in black with scan direction indicated by the arrow. Red lines show the CV in the range of the first oxidation process. (b) SWV of HMPD (pulse amplitude = 50 mV, pulse width = 50 ms, step potential = 5 mV). Peak potentials are indicated. (c) CV of OMPD in 0.1 M TBAP/CH_3CN (scan rate = 100 mV s^{-1}). Two successive scans are shown in black with scan direction indicated by the arrow. Red lines show the CV in the range of the first oxidation process. (d) SWV of OMPD (pulse amplitude = 50 mV, pulse width = 50 ms, step potential = 5 mV). Peak potentials are indicated.

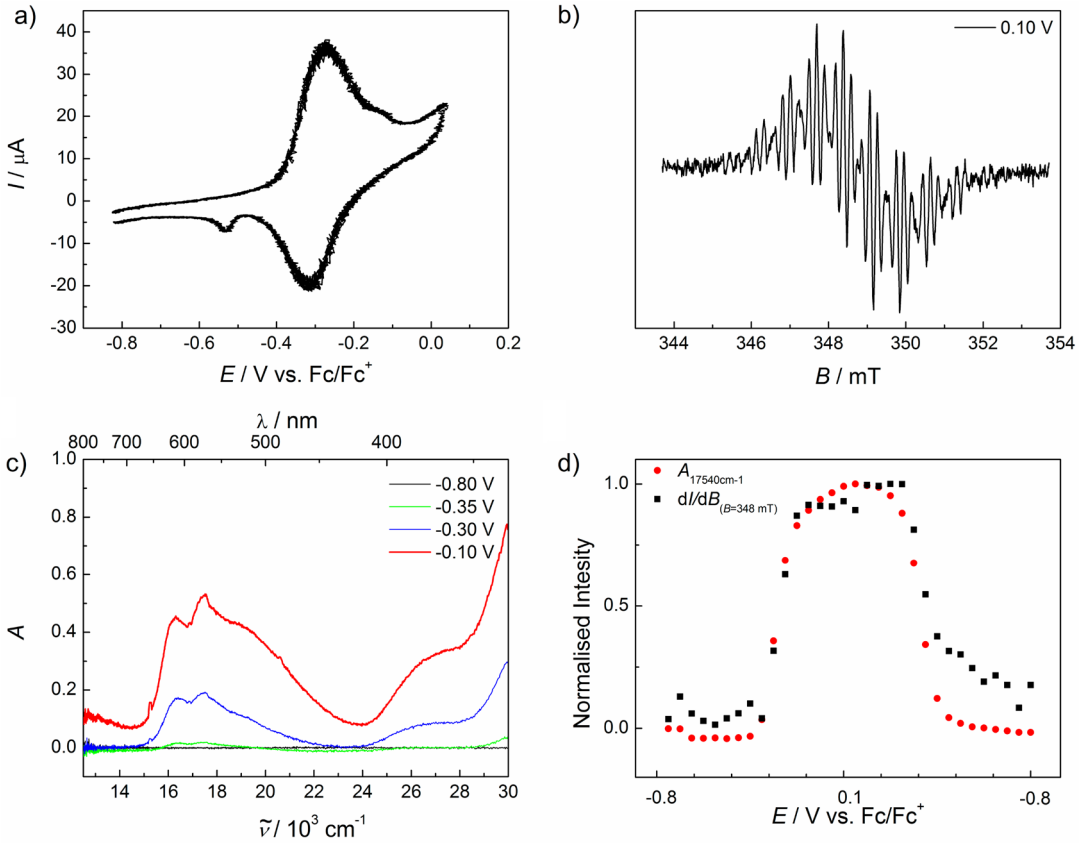

Figure 2. (a) Cyclic voltammogram from the in situ EPR/UV−vis spectroelecrochemical oxidation of HMPD 0.1 M TBAP/CH_3CN (scan rate = 2.7 mV s^{-1}). (b) EPR spectrum detected during the oxidation of HMPD in the potential region of the first ($2e^-$) oxidation step. (c) Selected difference UV−vis spectra detected during the oxidation of HMPD in the potential region of the first ($2e^-$) oxidation step. (d) Potential dependences of the UV−vis and EPR signals.

3. RESULTS AND DISCUSSION

Figure 1 shows the cyclic voltammograms (CVs) and the square-wave voltammograms (SWVs) of HMPD (CV, Figure 1a; SWV, Figure 1b) and OMPD (CV, Figure 1c; SWV, Figure 1d) recorded in 0.1 M TBAP/CH_3CN system using a Pt working electrode. Two successive scans were recorded in the CV with the scan direction indicated by the arrow. Square-wave voltammetry reveals the peak potentials.

Two reversible oxidation waves were observed in the potential range studied, with oxidation potentials typical for the charging of the PD core [e.g., −0.280 and 0.295 V vs Fc/Fc^+ in *N,N,N′,N′*-tetramethyl-*p*-phenylenediamine (TMPD)].[35] The shape of the volammetric peak in the region of the first

dx.doi.org/10.1021/jp3104358 | J. Phys. Chem. A 2013, 117, 1439−1448

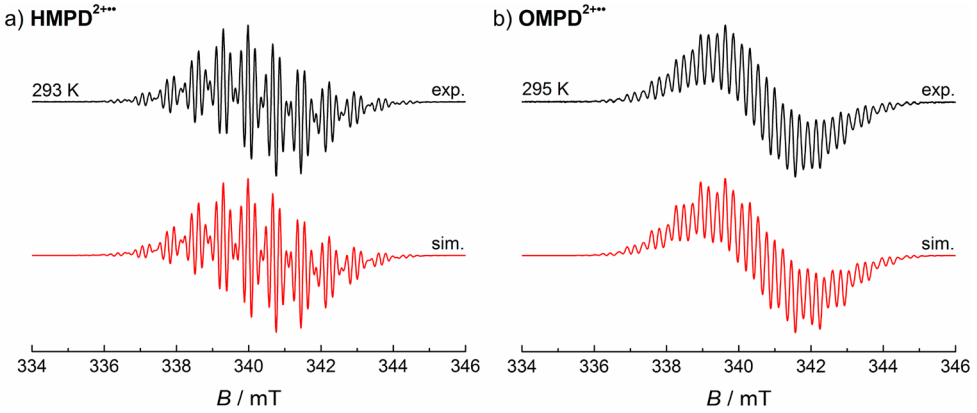

Figure 3. EPR spectra of (a) $HMPD^{2+\bullet\bullet}$ obtained by the oxidation of HMPD (solvent, methanol; oxidant, 2 equiv of PIFA, T = 293 K) and (b) $OMPD^{2+\bullet\bullet}$ obtained by the oxidation of OMPD (solvent, methanol; oxidant, 2 equiv of PIFA, T = 295 K), together with their simulations. The corresponding data are summarized in Table 1.

oxidation process is slightly deformed and points to a two-electron ($2e^-$) transfer, where the second electron is only slightly harder to remove than the first. The current transferred during the second oxidation peak is of a similar magnitude, and thus, this process also represents a $2e^-$ transfer.

As shown in Figure 1c,d, the CV and the SWV of OMPD are closely related to those of HMPD but with a somewhat larger separation between potentials for the first and second electron transfers.

To gain a better insight into the redox reactions, we performed in situ electrochemical oxidations in the cavity of the EPR spectrometer with the simultaneous detection of the EPR and UV−vis spectra. Panels b and c of Figure 2 show the EPR and UV−vis spectra, respectively, of HMPD recorded during the potential sweep in the region of the first oxidation process ($2e^-$). As both of these signals reached the highest intensity at the scan reverse potential of approximately 0.1 V vs Fc/Fc^+ (Figure 2d), they can be clearly assigned to the $HMPD^{2+\bullet\bullet}$ diradical dication. In principle, the spectrum of the mono-charged $HMPD^{+\bullet}$ should also be recorded during the experiment mainly in the potential region of the onset of the oxidation peak. However, we were not able to assign the peaks unambigously because of the very small potential difference for the first and second electron transfers and relatively low signal-to-noise ratio caused by the small surface of the working electrode.

Analogously, anodic oxidation of OMPD led to signals attributable to the dication $OMPD^{2+\bullet\bullet}$, being identical to those prepared by chemical oxidation with a 2-fold excess of PIFA in methanol (Figure 3b).

Spectroelectrochemical investigations provided only the information on the HMPD dication, as the data on the HMPD monocation could not be clearly distinguished owing to overlapping signals. Therefore, we decided to utilize chemical oxidation. In the first stage, $HMPD^{2+\bullet\bullet}$ was prepared by reacting HMPD with 2 equiv of PIFA. The corresponding EPR spectrum (solvent methanol) shown in Figure 3a is virtually identical to that obtained by anodic oxidation (Figure 2b). The simulation of the spectrum revealed the coupling of the unpaired electron with two equivalent nitrogen nuclei (a_N = 0.69 mT) and three sets of hydrogens, a_H = 0.69, 0.20, and 0.38 mT for 9, 4, and 2 equivalent or almost equivalent hydrogens, respectively (Table 1). The hyperfine data derived from the EPR spectrum obtained from OMPD under compatible conditions (Figure 3b, Table 1) are very similar. Although the methyl groups adjacent to the nitrogen atoms are symmetrically non-equivalent, matching EPR simulations can be obtained by using identical a_{HCH_3} values for these nine hydrogens. However small differences (<0.05 mT) between the coupling constants of the protons in these three methyl groups within the experimental line width can not be excluded.

Table 1. Hyperfine Coupling Constants (mT) and g factors of $HMPD^{2+\bullet\bullet}$ and $OMPD^{2+\bullet\bullet}$ Determined by Simulation of the Experimental EPR Spectra Recorded in Methanol at 293 and 295 K, Respectively[a]

	$HMPD^{2+\bullet\bullet}$	$OMPD^{2+\bullet\bullet}$
a_N(2N)	0.666(9)	0.654(9)
a_{HCH_3}(9H)	0.698(9)	0.690(9)
a_{HCH_2}(1H)	0.384(5)	0.432(8)
a_{HCH_2}(1H′)	0.370(8)	0.325(9)
a_{Harom}(4 H)	0.196(7)	0.195(9)
g factor	2.0030(1)	2.0031(1)

[a]Numbers in parentheses indicate uncertainty margins based on the simulation data, yielding compatible correlations with experiment.

The values of the isotropic hyperfine coupling constants are typical for Wurster-type radicals with a_N and a_{HCH_3} of the adjacent methyl groups of ca. 0.7 mT and a_{Harom} of 0.198 mT.[35] This reveals that the dication $HMPD^{2+\bullet\bullet}$ (and $OMPD^{2+\bullet\bullet}$) has to be regarded as two individual PD moieties covalently connected; that is, each of the two unpaired electrons of the diradical dication is localized at one individual PD core and constitutes a doublet−doublet state, with negligible exchange interaction. We, therefore, presume that these dications are predominately arranged as an extended conformation, because a π-stacked conformation would either show an overall singlet state or a triplet state, not detectable in fluid solution. Indeed, the variable-temperature studies shown below indicate that π-stacked conformation can be populated and that they lead to a decrease of the doublet character.

The shapes of the EPR spectras of $HMPD^{2+\bullet\bullet}$ and $OMPD^{2+\bullet\bullet}$ did not vary substantially when the temperature was varied; at low temperatures, a slight broadening of the lines was observed, presumably owing to the higher viscosity of the solvent and slight variations of the coupling constants (see the Supporting Information). The most remarkable change

dx.doi.org/10.1021/jp3104358 | J. Phys. Chem. A 2013, 117, 1439−1448

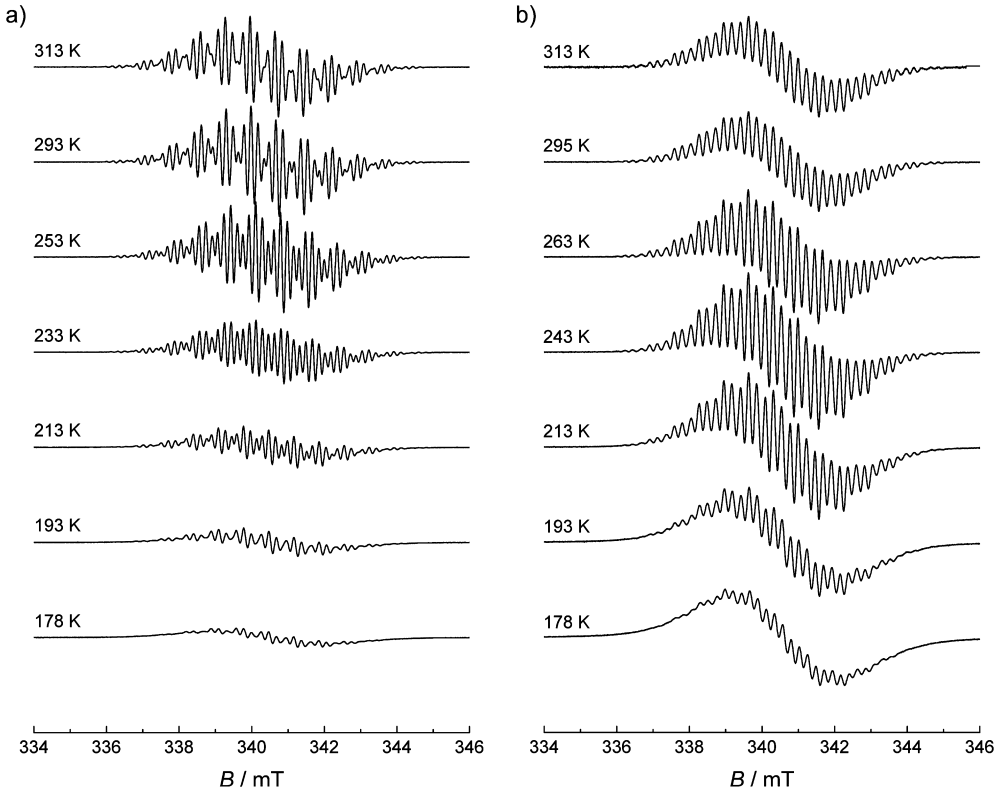

Figure 4. Variable-temperature EPR spectra of (a) $HMPD^{2+\bullet\bullet}$ and (b) $OMPD^{2+\bullet\bullet}$ obtained by the oxidation of 2 mM HMPD methanol solution with 4 mM PIFA.

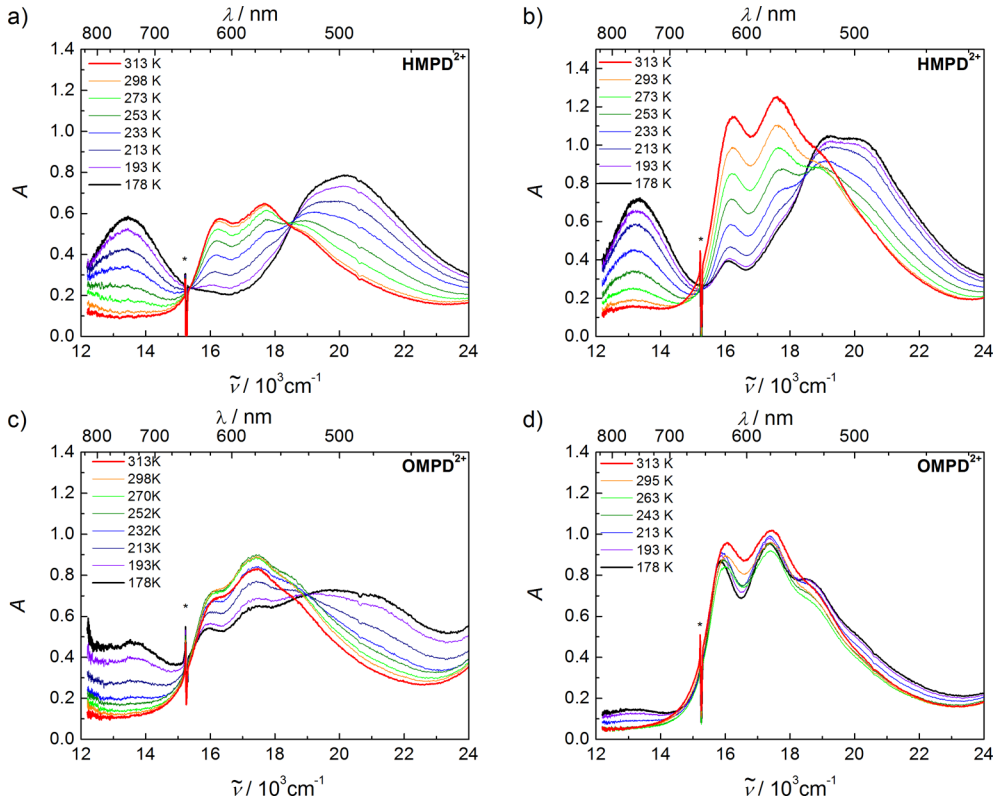

Figure 5. Variable-temperature (VT) UV−vis spectra of (a) 1 mM $HMPD(SbF_6)_2$ recorded in methanol during an in situ EPR/UV−vis experiment, (b) $HMPD^{2+\bullet\bullet}$ obtained by the oxidation of 2 mM HMPD with 4 mM PIFA recorded during an in situ EPR/UV−vis experiment (see panel a), (c) 1 mM $OMPD(SbF_6)_2$ recorded during an in situ EPR/UV−vis experiment, and (d) $OMPD^{2+\bullet\bullet}$ obtained by the oxidation of 2 mM OMPD with 4 mM PIFA recorded during an in situ EPR/UV−vis experiment (see panel b). The asterisk (*) marks a spectrometer artifact.

dx.doi.org/10.1021/jp3104358 | J. Phys. Chem. A 2013, 117, 1439−1448

however was a distinct variation of the EPR spectral intensity, as shown in Figure 4.

The behavior of the EPR spectrum is reflected in the optical spectra of $HMPD^{2+\bullet\bullet}$ and $OMPD^{2+\bullet\bullet}$, which are exceptionally temperature-sensitive (Figure 5). The spectrum observed at higher temperature [characterized by a single band with a maximum at 565 nm (17700 cm^{-1})] resembles that of the previously studied non-π-stacked paracyclophane $\mathbf{1(iPr)}^{2+}$.[17,18] On the other hand, the spectrum observed at low temperature, (characterized by two bands with maxima at 500 and 750 nm (20000 and 13333 cm^{-1}) is similar to that of π-stacked $\mathbf{1(Me)}^{2+}$.[17,18] The two isosbestic points at 540 and 650 nm (18520 and 15380 cm^{-1}) indicate a clean conversion of one form to the other in a single chemical process. The recorded UV–vis spectra thus monitor the equilibrium between the extended and π-stacked conformations of $HMPD^{2+\bullet\bullet}$, as illustrated in Scheme 2.

Scheme 2. Equilibrium of the π-Stacked and Extended Conformations of $HMPD^{2+\bullet\bullet}$

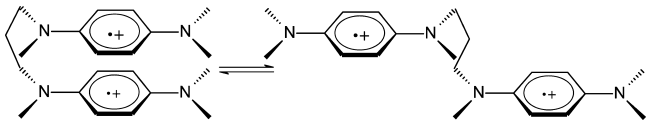

The conformational change explains the variable-temperature EPR and UV–vis spectra shown in Figures 4 and 5. At the higher temperatures, the extended form of the dications, with its EPR-visible double–doublet state, dominates. Here, the two unpaired electrons are localized on the individual $PD^{+\bullet}$ rings, which are well separated and have little or no mutual interaction. With decreasing temperature, the π-stacked conformation becomes more preferred, and the $PD^{+\bullet}$ rings get closer together. The π-stacked conformation is a diamagnetic singlet state (or a triplet state, not detectable in fluid solution), causing a decrease in the EPR intensity upon cooling.

This interpretation is consistent with the far lower temperature required to observe intermolecular π-stacking of monomeric $TMPD^{+\bullet}$ in the optical[10,36,37] and EPR[38] spectra at less than 190 K. Moreover, we found $HMPD^{2+\bullet\bullet}$ to be π-stacked also in the solid state.

Two SbF_6^- anions, one $HMPD^{2+\bullet\bullet}$ dication, and two CH_3CN solvent molecules were established in the asymmetric unit of the $HMPD(SbF_6^-)_2$ single crystal by the X-ray analysis. The crystal was an inversion twin with a 75%/25(3)% component ratio. The PD units were stacked in parallel centrosymmetric positions with an all-gauche NCCC twist angle conformation. Accordingly, the nonbonded distances between the pairs N1···N4 and N2···N3 were almost matching (difference of 0.18 Å; see Figure 6). The dication appears to represent the average of three different orientations in the lattice, reflecting the broad conformational flexibility of the single bridged PD dimer (see the Supporting Information). Numerous restraints and constraints were used to ensure chemically reasonable and computationally stable refinement. The central carbon atom of the bridge is disordered over three positions. In two conformations, the bridge is present at the N2/N3 site of the molecule [N–N separation 3.010(7) Å] in opposite orientation and 45.6(8)% and 34.6(7)% abundances, respectively. The remaining 19.8(4)% constitutes a geometry with the bridge at the N1/N4 end and a slightly longer N–N

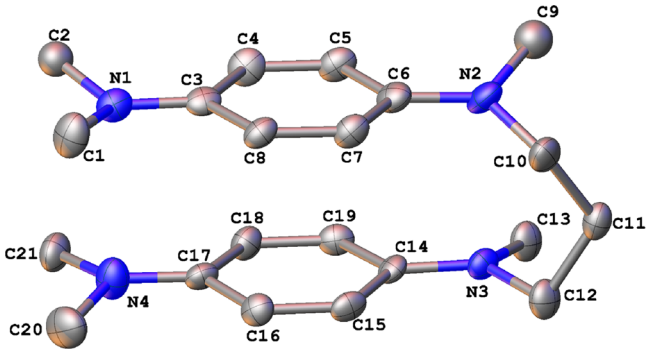

Figure 6. Most-abundant $HMPD^{2+}$ geometry in the [$HMPD(SbF_6)_2(CH_3CN)_2$] crystal structure. (Counterions, solvent molecules, H atoms, and minor components of the bridge disorder are omitted for clarity.)

separation of 3.188(8) Å. Some geometrical parameters obtained from the crystal structure are summarized in Table 2.

Table 2. Some Structural Parameters for the $HMPD^{2+}2SbF_6^-$ X-ray Structure

compound	$HMPD^{2+\bullet}2(SbF_6^-)$
NCCC conformations	gg,gg
dication symmetry	C_s
d_1(N2,N3) (Å)	3.010(7)
d_2(N1,N4) (Å)	3.188(8)
d_1(C6,C14)[a] (Å)	3.106(2)
d_2(C3,C17)[a] (Å)	3.189(2)
d_1(C7,C15)[b] (Å)	3.176(3)
d_2(C8,C16)[b] (Å)	3.224(3)
d(mean C_6 planes) (Å)	3.120(1)
PD ring displacement[c] (Å)	0.59
NCCC twists (deg)	−71.1,67.6

[a]Distance between pairs of quaternary ring carbons. [b]Distances between the closest ring CH carbons. [c]measured perpendicular to the average C_6 plane.

We initially made $OMPD^{2+\bullet\bullet}$ expecting a *gem*-dimethyl Thorpe–Ingold effect,[39] which favors conformations that make the X groups on many $XCH_2CMe_2CH_2X$ compounds lie closer in space than for a trimethylene bridge. This would lead to a preference for the π-stacked conformation, but instead, we found that it is clearly less prevalent for $OMPD^{2+\bullet\bullet}$ than for $HMPD^{2+\bullet\bullet}$. Because only a small decrease in the UV–vis feature attributable to the extended conformation and only a small increase in the pair of features attributable to the π-stacked conformation were observed as the temperature was lowered (compare Figure 5b,d), it is clear that the π-stacked conformation of $OMPD^{2+\bullet\bullet}$ is instead more difficult to form than it is for $HMPD^{2+\bullet\bullet}$. As illustrated in Figure 5a,b, the π-stacking dimerization process is sensitive to the counterions. With the same temperature gradient, the conformational change was more pronounced in the presence of SbF_6^- (Figure 5a) than with CF_3COO^- (Figure 5b).

Temperature dependence is also a common feature in the spectra of the monocations. However, the background of this phenomenon is distinctly different from that of the dications.

Figure 7 shows the EPR spectra obtained by the chemical oxidation of HMPD and OMPD using substoichiometric oxidant. These spectra are significantly different from those of

dx.doi.org/10.1021/jp3104358 | J. Phys. Chem. A 2013, 117, 1439–1448

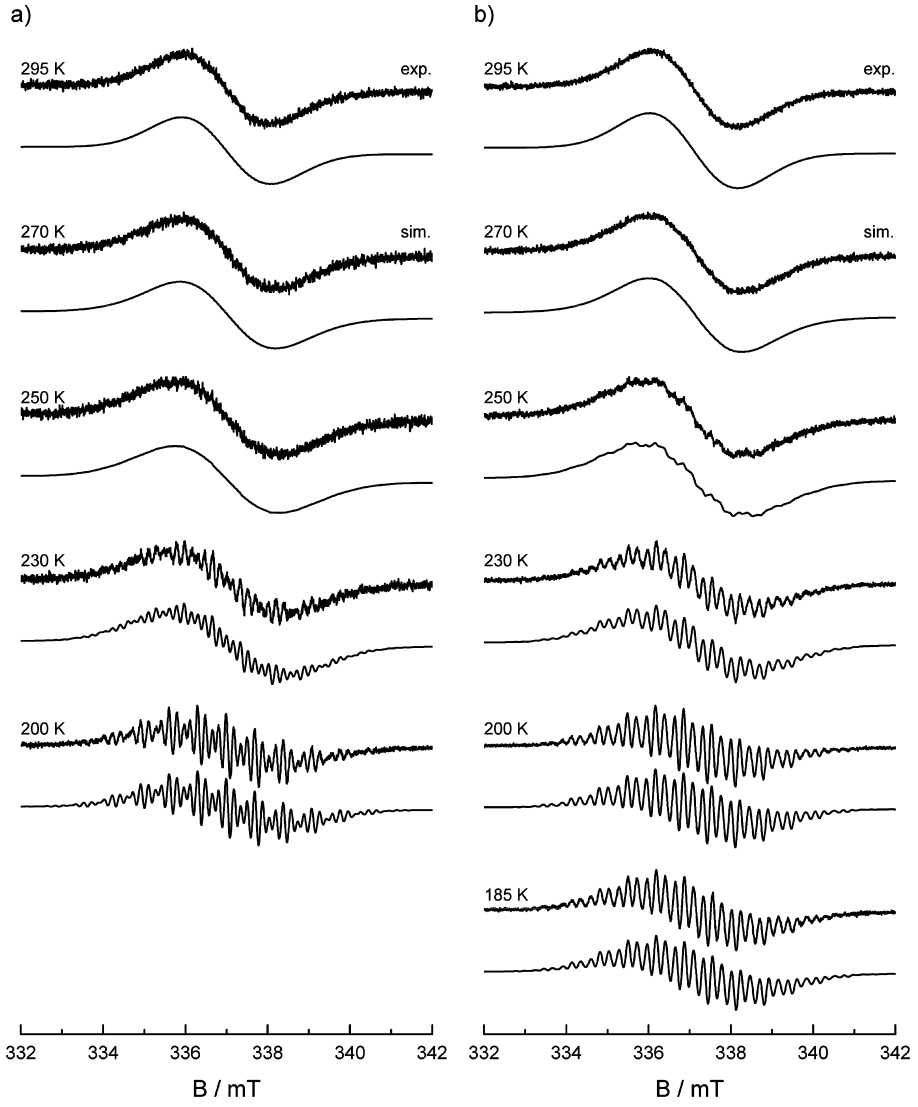

Figure 7. Normalized variable-temperature EPR spectra of (a) $HMPD^{+\bullet}$ obtained by oxidation of HMPD (solvent, methanol; oxidation with PIFA in stoichiometric deficiency) and (b) $OMPD^{+\bullet}$ obtained by oxidation of OMPD (solvent, CH_2Cl_2; oxidation with PIFA in stoichiometric deficiency), together with their simulations using EasySpin.

Table 3. Hyperfine Data and Rate Constants Used to Simulate the VT EPR Spectra of the Radical Monocations $HMPD^{+\bullet}$ and $OMPD^{+\bullet}$[a]

	a^b (mT)				k (MHz)		
	$OMPD^{+\bullet}$		$HMPD^{+\bullet}$		$OMPD^{+\bullet}$		$HMPD^{+\bullet}$
	CH_2Cl_2	CH_3OH	CH_3OH	T (K)	CH_2Cl_2	CH_3OH	CH_3OH
a_N(2N)	0.667(9)	0.671(9)	0.673(9)	185	0.5		
a_{HCH_3}(9H)	0.697(9)	0.692(9)	0.698(9)	200	2.0	0.2	1.6
a_{HCH_3}(4H)	0.189(5)	0.191(3)	0.202(2)	230	11.9		11.4
a_{Harom}(1H)	0.295(4)	0.307(4)	0.330(5)	250	33.0	3.6	41.2
a_{HCH_2}(1H′)	0.440(5)	0.441(5)	0.399(6)	270	116.3	15.2	88.4
				295	316.0	70.2	253.7

[a]Numbers in parentheses indicate uncertainty margins based on the simulation data, yielding compatible correlations with experiment. [b]a values are shown for first site of the two-site exchange model; exchange of all nuclei with identical second site with all a = 0 mT was considered.

$HMPD^{2+\bullet\bullet}$ and $OMPD^{2+\bullet\bullet}$ and substantially temperature-dependent.

Because the experimental conditions described above favor the formation of a monocation, the latter EPR signal is assigned to the radical monocation $HMPD^{+\bullet}$. This was confirmed in an additional experiment where an excess of neutral HMPD was added to a solution containing $HMPD^{2+\bullet\bullet}$. Because of the comproportionation equilibrium

$$HMPD^{2+\bullet\bullet} + HMPD \rightleftharpoons 2HMPD^{+\bullet} \quad (1)$$

dx.doi.org/10.1021/jp3104358 | J. Phys. Chem. A 2013, 117, 1439−1448

the $HMPD^{+\bullet}$ radical cation was populated leading to the same EPR signal as shown in Figure 7a.

Remarkably, the dependencies of the EPR spectral shapes for $HMPD^{+\bullet}$ and $OMPD^{+\bullet}$ are distinctly different from those observed for the dications. As shown in Figure 7, the spectral shape changed dramatically with the change in temperature. In this latter case, these phenomena can be traced back to dynamic changes occurring at the hyperfine time scale. Although EPR spectra with coupling constants typical for PD cation radicals were observed at lower temperatures, at room temperature, a narrower signal with loss of hyperfine structure was observed. This was caused by the electron exchange between two PD units (fast on the EPR time scale at 295 K, but slow at 185 K). These dynamics are dependent on the solvent and the counterion, illustrated by the different dynamics detected in different solvents (see Table 3 and the Supporting Information). The simulations of the experimental spectra can be accomplished with chemical exchange in terms of "hole hopping" between two equivalent PD units. Using the Arrhenius relationship, an activation energy of 26.3 ± 0.6 $kJ{\cdot}mol^{-1}$ for $HMPD^{+\bullet}$ was calculated in methanol (Figure 8); the corresponding value for $OMPD^{+\bullet}$ was 29.3 ± 3.0 $kJ{\cdot}mol^{-1}$ in methanol and 26.0 ± 0.8 $kJ{\cdot}mol^{-1}$ in CH_2Cl_2.

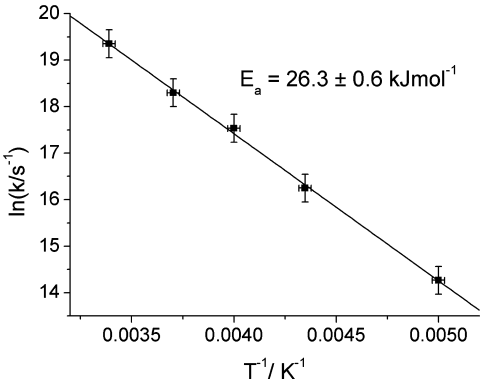

Figure 8. Arrhenius plot for hole-hopping rate constants derived from the simulations of the variable-temperature EPR spectra of $HMPD^{+\bullet}$.

The electron transfer between the two PD rings is fast on the time scale of the EPR experiments at room temperature but does not affect the UV–vis spectra. Indeed, the room-temperature UV–vis spectrum of $HMPD^{+\bullet}$ (Figure 9, blue line) is typical for Wurster's radical cation,[8,35,40,41] showing that, at the time scale of the UV–vis experiments (which is much shorter than for the EPR experiments), the unpaired electron is localized on a single PD unit. The spectrum is also similar to that of the $HMPD^{2+\bullet\bullet}$ (Figure 9, purple line), where the two unpaired electrons reside in separated PD rings of the extended conformation.

CONCLUSIONS

The high conformational freedom in the monobridged PD derivatives HMPD and OMPD causes substantially higher flexibility and shows temperature-dependent dynamics, as well as solvent and counterion dependence of the oxidized states. For example, in $HMPD^{2+\bullet\bullet}$, the ratio of π-stacked to extended conformations present is highly temperature-sensitive, with the π-stacked conformation predominating at low temperature and the extended conformation prevailing above room temperature. This makes the optical absorption spectrum unusually temperature-sensitive, similarly to the EPR spectrum where the π-stacked conformation does not contribute to the EPR intensity. Changing the single bridge from $(CH_2)_3$ to $CH_2CMe_2CH_2$ in the octamethyl-substituted compound $OMPD^{2+\bullet\bullet}$ causes considerably less of the π-stacked conformation to be present at low temperature than for $HMPD^{2+\bullet\bullet}$, presumably because of steric interactions with the methyl groups of the bridge. Moreover, the π-stacked/extended conformation equilibrium of both dications is influenced by the counterions present in the solution.

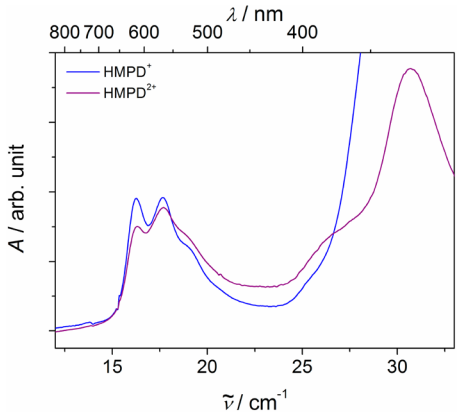

Figure 9. UV–vis spectra of $HMPD^{+\bullet}$ (blue) and $HMPD^{2+\bullet\bullet}$ (purple) in CH_2Cl_2 solution. The off-scale UV absorption band in the spectrum of $HMPD^{+\bullet}$ originates from the unreacted neutral HMPD.

Rather different temperature dependence was observed in the EPR spectra of the radical cations (for both $HMPD^{+\bullet}$ and $OMPD^{+\bullet}$) and could be rationalized considering the "hole hopping" (electron exchange) between the PD rings, fast on the EPR time scale at room temperature but slowed upon cooling. The rate of this process was found to be solvent-dependent and also influenced by the substitution on the $(CH_2)_3$ bridge.

This behavior illustrates the subtle interplay of several factors influencing the electronic properties of mixed compounds and states.[42,43]

ASSOCIATED CONTENT

Supporting Information

Variable-temperature (VT) EPR spectra of cations and dications with simulations, spectroelectrochemical data for the oxidation in the second oxidation step, and X-ray analysis data. This material is available free of charge via the Internet at http://pubs.acs.org.

AUTHOR INFORMATION

Corresponding Author

*Tel.: +43-316-873-32228 (M.Z.), +43-316-873-32220 (G.G.). Fax.: +43-316-873-32202 (M.Z.), +43-316-873-32202 (G.G.). E-mail: zalibera.m@gmail.com (M.Z.), g.gescheidt-demner@tugraz.at (G.G.).

Notes

The authors declare no competing financial interest.

ACKNOWLEDGMENTS

The financial support of NSF Grant CHE-0647719 (S.F.N.), SGA (Project VEGA 1/0289/12), and the Jubilee Fellowship for Post-Doctoral Candidates (SK-AT, Action Austria-Slovakia), the Stiftung Pro Bono and TU Graz to M.Z. are duly

acknowledged. S.S. thanks the University of Washington for financial support.

REFERENCES

(1) Zhu, C.; Liu, L.; Yang, Q.; Lv, F.; Wang, S. *Chem. Rev.* **2012**, *112* (8), 4687−4735.
(2) Wenger, O. S. *Chem. Soc. Rev.* **2012**, *41* (10), 3772−3779.
(3) Wang, C.; Dong, H.; Hu, W.; Liu, Y.; Zhu, D. *Chem. Rev.* **2011**, *112* (4), 2208−2267.
(4) Onitsch, C.; Rosspeintner, A.; Angulo, G.; Griesser, M.; Kivala, M.; Frank, B.; Diederich, F.; Gescheidt, G. *J. Org. Chem.* **2011**, *76* (14), 5628−5635.
(5) Moriuchi, T.; Hirao, T. *Acc. Chem. Res.* **2011**, *45* (3), 347−360.
(6) Guo, S.; Wang, E. *Acc. Chem. Res.* **2011**, *44* (7), 491−500.
(7) Zic, M. *J. Electroanal. Chem.* **2009**, *635* (1), 29−38.
(8) Albrecht, A. C.; Simpson, W. T. *J. Am. Chem. Soc.* **1955**, *77* (17), 4454−4461.
(9) Grilj, J.; Laricheva, E. N.; Olivucci, M.; Vauthey, E. *Angew. Chem., Int. Ed.* **2011**, *50* (19), 4496−4498.
(10) Nakayama, S.; Suzuki, K. *Bull. Chem. Soc. Jpn.* **1973**, *46* (12), 3694−3698.
(11) Gleiter, R.; Schafer, W. *Acc. Chem. Res.* **1990**, *23* (11), 369−375.
(12) Hoffmann, R. *Acc. Chem. Res.* **1971**, *4* (1), 1−9.
(13) Paddonrow, M. N. *Acc. Chem. Res.* **1982**, *15* (8), 245−251.
(14) Ito, A.; Sakamaki, D.; Ichikawa, Y.; Tanaka, K. *Chem. Mater.* **2011**, *23* (3), 841−850.
(15) Szeghalmi, A. V.; Erdmann, M.; Engel, V.; Schmitt, M.; Amthor, S.; Kriegisch, V.; Noell, G.; Stahl, R.; Lambert, C.; Leusser, D.; Stalke, D.; Zabel, M.; Popp, J. *J. Am. Chem. Soc.* **2004**, *126* (25), 7834−7845.
(16) Grossmann, B.; Heinze, J.; Moll, T.; Palivan, C.; Ivan, S.; Gescheidt, G. *J. Phys. Chem. B* **2004**, *108* (15), 4669−4672.
(17) Nelsen, S. F.; Li, G.; Schultz, K. P.; Tran, H. Q.; Guzei, I. A.; Evans, D. H. *J. Am. Chem. Soc.* **2008**, *130* (35), 11620−11622.
(18) Jalilov, A. S.; Li, G.; Nelsen, S. F.; Guzei, I. A.; Wu, Q. *J. Am. Chem. Soc.* **2010**, *132* (17), 6176−6182.
(19) Hohenstein, E. G.; Sherrill, C. D. *WIREs Comput. Mol. Sci.* **2012**, *2*, 304−326.
(20) Ehrlich, S.; Möllmann, J.; Grimme, S. *Acc. Chem. Res.*, published online Jun 15, 2012, 10.1021/ar3000844.
(21) Rosspeintner, A.; Griesser, M.; Matsumoto, I.; Teki, Y.; Li, G.; Nelsen, S. F.; Gescheidt, G. *J. Phys. Chem. A* **2010**, *114* (23), 6487−6492.
(22) Jalilov, A. S.; Nelsen, S. F.; Guzei, I. A.; Wu, Q. *Angew. Chem., Int. Ed.* **2011**, *50* (30), 6860−6863.
(23) Petrova, J. N.; Romanova, J. R.; Madjarova, G. K.; Ivanova, A. N.; Tadjer, A. V. *J. Phys. Chem. B* **2011**, *115* (14), 3765−3776.
(24) Kim, J.; Park, S.; Scherer, N. F. *J. Phys. Chem. B* **2008**, *112* (49), 15576−15587.
(25) Torf, S. F.; Khromov-Borisov, N. V.; Cherepanova, V. P. *Pharm. Chem. J.* **1973**, *7* (9), 562−565.
(26) Rapta, P.; Bartl, A.; Gromov, A.; Stasko, A.; Dunsch, L. *ChemPhysChem* **2002**, *3* (4), 351−356.
(27) Petr, A.; Dunsch, L.; Neudeck, A. *J. Electroanal. Chem.* **1996**, *412* (1−2), 153−158.
(28) Duling, D. R. *J. Magn. Reson.* **1994**, *104* (2), 105−110.
(29) Stoll, S.; Schweiger, A. *J. Magn. Reson.* **2006**, *178* (1), 42−55.
(30) Binsch, G. *J. Am. Chem. Soc.* **1969**, *91* (6), 1304−1309.
(31) Heinzer, J. *Mol. Phys.* **1971**, *22* (1), 167−177.
(32) Bain, A. D. *Prog. Nucl. Magn. Reson. Spectrosc.* **2003**, *43* (3−4), 63−103.
(33) Sheldrick, G. M. *Acta Crystallogr. A: Found. Crystallogr.* **2007**, *64* (1), 112−122.
(34) Dolomanov, O. V.; Bourhis, L. J.; Gildea, R. J.; Howard, J. A. K.; Puschmann, H. *J. Appl. Crystallogr.* **2009**, *42* (2), 339−341.
(35) Grampp, G.; Kelterer, A. M.; Landgraf, S.; Sacher, M.; Niethammer, D.; Telo, J. P.; Dias, R. M. B.; Vieira, A. *Monatsh. Chem.* **2005**, *136* (4), 519−536.
(36) Hausser, K. H.; Murrell, J. N. *J. Chem. Phys.* **1957**, *27* (2), 500−504.
(37) Uemura, K.; Nakayama, S.; Seo, Y.; Suzuki, K.; Ooshika, Y. *Bull. Chem. Soc. Jpn.* **1966**, *39* (6), 1348.
(38) Kawamori, A. H., A.; Joo, N.; Suzuki, K.; Ooshika, Y. *J. Chem. Phys.* **1966**, *44*, 4363.
(39) Beesley, R. M.; Ingold, C. K.; Thorpe, J. F. *J. Chem. Soc.* **1915**, *107*, 1080−1106.
(40) Zalibera, M.; Rapta, P.; Gescheidt, G.; Christensen, J. B.; Hammerich, O.; Dunsch, L. *J. Phys. Chem. C* **2011**, *115* (10), 3942−3948.
(41) Rapta, P.; Dunsch, L. *J. Electroanal. Chem.* **2001**, *507* (1−2), 287−292.
(42) Mechouet, M.; Perruchot, C.; Maurel, F.; Aeiyach, S.; Bucher, C.; Chardon, S.; Jouini, M. *J. Phys. Chem. A* **2012**, *116* (3), 970−978.
(43) Hankache, J.; Wenger, O. S. *Chem. Rev.* **2011**, *111* (8), 5138−5178.